ELSEVIER

Contents lists available at ScienceDirect

# **Biological Conservation**

journal homepage: www.elsevier.com/locate/biocon



# Incorporating caudate species susceptibilities and climate change into models of *Batrachochytrium salamandrivorans* risk in the United States of America

Matthew Grisnik <sup>a</sup>, Matthew J. Gray <sup>b</sup>, Jonah Piovia-Scott <sup>c</sup>, Edward Davis Carter <sup>b</sup>, William B. Sutton <sup>a,\*</sup>

- <sup>a</sup> Wildlife Ecology Laboratory, Department of Agricultural and Environmental Sciences, Tennessee State University, Nashville, TN 37209, USA
- <sup>b</sup> Center for Wildlife Health, Department of Forestry, Wildlife and Fisheries, University of Tennessee, Knoxville, TN 37996, USA

### ARTICLE INFO

### Keywords: Fungus Climate change Disease Emerging pathogens Introduction risk Landscape

### ABSTRACT

Worldwide, amphibians are threatened by several factors including climate change and pathogens. One emerging fungal pathogen, *Batrachochytrium salamandrivorans* (Bsal) has caused die-offs of European salamander populations, representing a conservation concern for hotspots of salamander diversity in the United States of America (U.S.A.). While Bsal has not been detected in the U.S.A., previous work has suggested high invasion potential. As species susceptibility to Bsal is temperature dependent, we expect climate change to impact Bsal risk, which has not been explored. Here, we used predicted changes in environmental conditions, species-specific susceptibility estimates, and novel approaches assessing introduction risks to estimate current and future Bsal invasion risk. To generate predictions, we used geospatial data representing introduction risks, species susceptibility, and climatic suitability. Across climatic scenarios, our models predicted greatest overall risk of Bsal emergence in the southeastern and northwestern U.S.A. Bsal climatic suitability was greatest in the northwest, whereas the greatest number of susceptible species was predicted in the southeast. Under future scenarios, we predicted that climatically suitable areas for Bsal will be reduced by 3–14 % under the most extreme climate model.

# 1. Introduction

Worldwide, amphibian populations are threatened by multiple stressors including anthropogenic disturbance, climate change, and emerging infectious diseases (Wake and Vredenburg, 2008). Of particular concern for amphibians are emerging fungal pathogens (e.g., DiRenzo and Grant, 2019), particularly those that cause chytridiomycosis. One of the fungal agents of chytridiomycosis, *Batrachochytrium dendrobatidis* (Bd), has been associated with the decline of many amphibian species (Scheele et al., 2019), though disentangling the impacts of Bd from other stressors is challenging (Lambert et al., 2020). The number of susceptible species to this pathogen, as well as its capability to cause extinctions, have led many to describe it as the worst vertebrate infectious disease in recorded history (Gascon et al., 2007).

More recently, a second fungal agent of chytridiomycosis, *Batrachochytrium salamandrivorans* (Bsal) has been identified and associated with localized and regional salamander die-offs in Europe (Martel et al., 2013). In addition to causing salamander population collapses, Bsal has been shown to retain virulence in the environment, reservoir species, and salamanders that have survived previous infection (Stegen et al., 2017), emphasizing its potential to have long-term effects on susceptible host populations. Evidence suggests that Bsal is endemic to East Asia, where the pathogen is documented in asymptomatic salamander populations and is hypothesized to have spread to Europe through the amphibian trade (Martel et al., 2014). With over 4 million amphibians imported into the U.S.A. every year and no requirement for animal health certificates (Grant et al., 2017), there is a considerable need to understand locations at greatest risk of Bsal invasion and potential

<sup>&</sup>lt;sup>c</sup> School of Biological Sciences, Washington State University, Vancouver, WA, USA

<sup>\*</sup> Corresponding author at: Wildlife Ecology Laboratory, Department of Agricultural and Environmental Sciences, Tennessee State University, 3500 John A Merritt Blvd, Nashville, TN 37209, USA.

E-mail addresses: mgrisnik@tnstate.edu (M. Grisnik), mgray11@utk.edu (M.J. Gray), jonah.piovia-scott@wsu.edu (J. Piovia-Scott), ecarte27@utk.edu (E.D. Carter), wsutton@tnstate.edu (W.B. Sutton).

consequences on native amphibian species. To date, Bsal has not been detected in North America (Waddle et al., 2020; Hill et al., 2021), however the spread of Bsal into North America is of concern as 48 % of described salamander species are endemic to North America (Amphibiaweb.com).

The total risk of disease outbreak can be summarized as a combination of two factors, specifically the introduction of a pathogen, and the consequences of that introduction (Richgels et al., 2016). There have been multiple hypothesized routes for the introduction of other fungal pathogens into North America. The first is through spillover from the wildlife trade, which is the current hypothesis for the origin of Bsal in Europe (Martel et al., 2014). This hypothesis is supported by detection of Bsal infection in commonly traded amphibians, as well as in European pet collections (Martel et al., 2014; Fitzpatrick et al., 2018). Thus, the greatest risk of Bsal introduction may be located near the greatest density of pet stores, and therefore pet amphibian consumers (Richgels et al., 2016). Alternatively, a second route is through fomite-mediated dispersal. For example, Pseudogymnoascus destructans, the fungal agent of white-nose syndrome, which is causing bat population die-offs across North America, is hypothesized to have been introduced from Europe through contaminated caving equipment (Leopardi et al., 2015). Hence, locations with high tourist visitation may have the greatest likelihood of Bsal invasion. To date, previous Bsal risk analyses (Moubarak et al., 2022; Yap et al., 2015; Richgels et al., 2016) have not considered both of these routes of human-mediated introduction to the U.S.A.

Once a pathogen has been introduced, the consequences of the introduction are likely an interaction of pathogen traits, host susceptibility, and environmental conditions – as emphasized in the epidemiological triangle (McNew, 1960; Fig. 1). In terms of pathogen traits, previous work has suggested that the Bd genotype has implications for disease outcomes, with some isolates showing reduced virulence (Refsnider et al., 2015). However, there is currently a lack of information on variation in Bsal virulence. Species-specific susceptibility to Bsal has been documented in salamander species worldwide, with responses varying from 100 % mortality to full infection resistance (Martel et al., 2014; Carter et al., 2020; Gray et al., 2023). This variability in species responses indicates that Bsal invasion risk in the U.S.A. is likely not

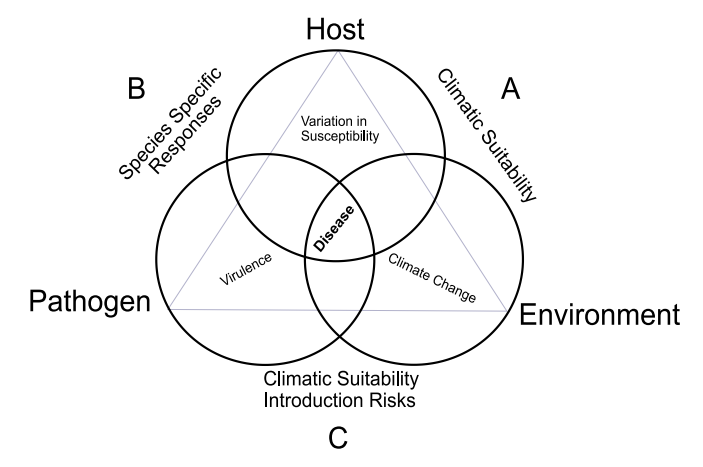


Fig. 1. Conceptual diagram of our modeling approach based on the epidemiological triangle (McNew, 1960). To generate a prediction of Bsal emergence risk, we incorporated the interactions among three factors, including host, pathogen, and favorable environment. To model the interaction between hosts and the environment (A), we used ecological niche modeling (ENM) to identify areas of suitability for each host species. We then evaluated the influence of climate change on the climatic suitability for hosts and the pathogen, which we incorporated through ENMs. To model the interaction between host and pathogen (B), we incorporated the variation in host susceptibility. Lastly the interaction between pathogen and environment (C) was incorporated by identifying areas (under both current and predicted climate models) of climatic suitability for Bsal.

uniform; areas with salamander assemblages made up of highly susceptible species represent a greater conservation risk than areas with resistant species.

Host environment, more specifically, climate can presumably impact pathogen invasion and pathogen emergence by affecting environmental suitability for the pathogen, as well as host tolerance, susceptibility, and distribution (Carter et al., 2021; Gallana et al., 2013). While our understanding of Bsal thermal preference on the landscape is lacking, previous work has shown that in vitro, Bsal has optimal growth between 10 and 15 °C, with a thermal maximum temperature of 25 °C (Martel et al., 2013). For host amphibians, the environmental temperature affects physiological processes such as immune function (Rollins-Smith, 2020). Additionally, previous work has suggested that temperature influences Bsal infection and mortality rates of Notophthalmus viridescens (Carter et al., 2021), which supports the importance of host, pathogen, and environmental interactions. Previous work has modeled the climatic suitability of Bsal in the U.S.A. using multiple methods (Moubarak et al., 2022; Yap et al., 2015), but these efforts have not considered future climate change scenarios. Climate change models for Bd climatic suitability suggest a northward shift in suitability for the pathogen in the Northern Hemisphere (Xie et al., 2016). Therefore, it is important not only to understand the interactions between pathogen and environment, but also understand how environmental change will influence Bsal emergence risks.

Our primary study objective was to evaluate Bsal invasion risk and potential consequences on resident amphibian populations in the U.S.A. at the ecoregion level, while taking into consideration: (1) possible routes of Bsal invasion, (2) susceptibility of resident species, (3) environmental suitability of Bsal, and (4) projected climate change. This work is essential to understand locations of greatest likelihood of Bsal invasion currently and in the future, which can be used to guide surveillance plans and respond to outbreaks if Bsal is introduced to the U.S. A.

# 2. Methods

# 2.1. Salamander species distribution modeling

To model the interactions between hosts and the environment (Fig. 1a), we employed an ecological niche modeling (ENM) approach in R 4.1.0 (R Core Team, 2021) to predict the climatic suitability for salamander species in the U.S.A. based on species accounts described on amphibiaweb.com. We obtained locality data for each salamander species (n = 204 species) from the Global Biodiversity Information Facility (GBIF; www.gbif.org/; citations in Supplemental File S1.1), VertNet (www.vertnet.org), and Biodiversity Information Serving Our Nation (BISON; www.bison.usgs.gov/#home) databases. To curate occurrence data, we removed duplicate occurrences, potential outliers, and occurrence records that were collected prior to 1970. Specifically, outliers were defined as occurrence points found outside a 50 km buffered International Union for Conservation of Nature (IUCN) species range map as completed in Sutton et al. (2015). Additionally, species with fewer than 30 occurrences were not included in further analyses (Wisz et al., 2008), resulting in the removal of 70 salamander species (Supplemental File S2.1). To reduce bias caused by oversampling at well-known locations (e.g., biological research stations, national parks, and sites near roads; Kramer-Schadt et al., 2013), we filtered samples within a 5 km radius (Sutton et al., 2015). Our final dataset included 134 salamander species, including 21 genera, and 8 families (Supplemental File S2.1).

For each salamander species evaluated, we used the Maximum Entropy algorithm (MaxEnt; Phillips et al., 2006; version 3.4.3) in the R package *ENMeval* (version 2.0.3; Kass et al., 2023) and the Random Forest (RF) algorithm within the R package *randomForest* (Liaw and Wiener, 2002) to determine the current and projected climatic suitability for the years 2050 and 2070. These machine learning algorithms were selected as they have been shown to outperform other regression-

based ENM methods (Elith et al., 2006). For MaxEnt models, previous work has suggested that modification of two parameters within MaxEnt, the regularization parameter and the feature class, increases model predictability (e.g. Anderson and Gonzalez, 2011). Therefore, we tested a combination of four feature classes (linear, linear quadratic, linear quadratic hinge, and hinge) as well as four regularization parameters (0.5, 1, 2, and 5). For some species, hinge feature classes were dropped as a modeling option due to inadequate model convergence. We then selected the model with the combination of regularization parameter and feature classes that produced the lowest AICc value (Warren and Seifert, 2011) for downstream analyses.

Both MaxEnt and RF approaches require background locations (i.e., pseudoabsences), therefore we used a bias file approach (e.g., Phillips and Dudik, 2008) to model climatic suitability for each salamander species. This approach helps to counteract bias that may be present within occurrence data points, as is common with data acquired from museum and other public databases (Phillips et al., 2009). We developed the bias file using locations for all salamander species in the U.S.A. and included geographic ranges for salamander species that extended into both Canada and Mexico using locality data downloaded from the GBIF, VertNet, and BISON databases. These occurrence points were then transformed into a kernel density map using a combination of the rasterize (raster package; Hijmans et al., 2013) and kde2d command (MASS package; Ripley et al., 2013) to generate a raster with an estimate of salamander survey effort in each raster cell. This layer was clipped to the 50 km buffered range of each focal species to limit background locations within the focal species range. The number of background points were model algorithm-specific, as previous work has suggested that the ratio of background points to occurrence points can influence model accuracy (Barbet-Massin et al., 2012). Specifically, following Barbet-Massin et al. (2012), we used 10,000 background points for MaxEnt models, and an equal number of background points to occurrence points for RF models. Background points were allocated following the kernel density distribution, with areas of relatively greater occurrence points receiving a greater allocation of background points.

Baseline (1970–2000) and projected climatic data were acquired from the Worldclim database (www.worldclim.org; Fick and Hijmans, 2017; version 2.1) at a 30 s resolution. We selected CMIP5 models despite the recent introduction of CMIP6 models due to the lack of availability of CMIP6 models at the 30 s resolution. These data represent 19 geospatial layers of bioclimatic variables that represent temperature and precipitation trends derived from global temperature and precipitation grids (Hijmans et al., 2005). To prevent model overparameterization, we removed climate layers that were correlated with a Pearson's correlation coefficient  $\geq$  0.75, while maintaining the variable of hypothesized importance (Sutton et al., 2015), which resulted in the inclusion of nine bioclimatic variables (Bio 2, Bio 3, Bio 5, Bio 7, Bio 8, Bio 9, Bio 15, Bio 17, Bio 19; Supplemental File S2.2). These same nine bioclimatic variables were included in future climate suitability predictions for all species.

We evaluated 12 projected Global Climatic Models (GCMs; Supplemental File S2.2) to model the projected climatic suitability for each species and reduce between-model variability (Lyons and Kozak, 2020; Wright et al., 2015). We selected 12 GCMs based on a clustering analysis conducted by Knutti et al. (2013). Specifically, we identified 12 clusters of similar models and randomly selected a single GCM within each cluster (Lyons and Kozak, 2020). To account for additional uncertainty in climatic projections, we used two Representative Concentration Pathways (RCPs), which included the RCP 4.5 and RCP 8.5 greenhouse gas scenarios. The RCPs are projected greenhouse gas emission scenarios into the year 2100 and represent the radiative forcing of greenhouse gases on future climate change (van Vuuren et al., 2011). The RCPs of 4.5 and 8.5 were selected as they represent a range of greenhouse gas emissions from moderate (RCP 4.5) to extreme (RCP 8.5) scenarios, similar to Sutton et al. (2015). This resulted in 97 climatic suitability models per species (n = 12,998 total models). For each salamander

species, we generated one current climatic suitability model, and four projected climatic suitability models. The four projected climatic suitability models were generated by averaging the 12 GCMs generated by both MaxEnt and RF within year (either 2050 or 2070) and RCP (either 4.5 or 8.5), resulting in four projected suitability models (RCP 4.5 at year 2050, RCP 4.5 at year 2070, RCP 8.5 at year 2070).

### 2.2. Batrachochytrium salamandrivorans climatic suitability prediction

To model the interactions between pathogen and the environment (Fig. 1c), we predicted the climatic suitability for Bsal within the U.S.A. by employing the same species distribution modeling framework as described above for both current and predicted (12 GCMs) climatic conditions (Section 2.1). We used 77 Bsal occurrence points from the native range in Asia as well as the introduced locations in Europe as published in Basanta et al. (2019) to estimate climatic suitability for Bsal. We followed the same modeling approaches outlined above using both the RF and MaxEnt algorithms. We selected background points at random from within a 50 km buffer for each occurrence location, as the overall native range of Bsal is unknown. As conducted with the salamander climatic suitability analysis, we used 10,000 background points for MaxEnt and the same number of background points as occurrence points (n = 77) for the RF analysis (Barbet-Massin et al., 2012). Once the model was generated for the climatic suitability in Asia and Europe, we projected this model onto the same bioclimatic variables throughout the U.S.A. to predict climatically suitable landscapes. To assess model fit, we used Area Under the Curve (AUC) estimates based on cross-validation of five subsampled replicates, as well as the true skill statistic (TSS) based on the maximum sensitivity plus specificity threshold.

To identify climatic conditions within the U.S.A that are highly dissimilar from conditions in the native and introduced range of Bsal, we used the mobility-oriented parity (MOP) analysis via the *kuenm* R package (Cobos et al., 2019). The MOP analysis creates multivariate distances between climatic variables at points in the native and introduced range (Asia and Europe) and climatic variables in the U.S.A. (Owens et al., 2013) and identifies areas of high extrapolation risk.

To obtain a broader view of Bsal climatic suitability across the U.S.A. and identify zones of concern, we used R to define quantiles of climatic suitability for the current Bsal climate suitability model (defined as Low, Medium Low, Medium High, and High). We then used these quantiles to determine how these categories changed for Bsal suitability across predicted climatic change scenarios, which was measured as relative change in suitability.

# 2.3. Predicting mortality and infection

To model the interaction between hosts and pathogen (Fig. 1b), we generated a raster layer that represented mortality and infection risk within salamander assemblages using data from laboratory studies that determined the percent mortality and infection of salamander species exposed to Bsal (Carter et al., 2020; Gray et al., 2023). For species in which we lacked laboratory infection and mortality data (n=99), we used a phylogenetic approach to predict mortality as conducted in Gray et al. (2023). Briefly, we used the function phyEstimate in the picante R package (Kembel et al., 2010), which uses known trait data to predict the ancestral trait for a phylogeny. The phylogeny used for salamanders was created from the Timetree database (timetree.org). When there were insufficient data to predict susceptibility based on phylogenetic relatedness (n=7; Supplemental File S2.1), we averaged species mortality and infection potential values from congenerics.

To determine how salamander susceptibility is distributed across the landscape, we multiplied the suitability scores from the averaged Max-Ent and RF models by the infection and mortality rates as described above. We then summed these layers across species to generate two separate models of accumulated infection and accumulated mortality for

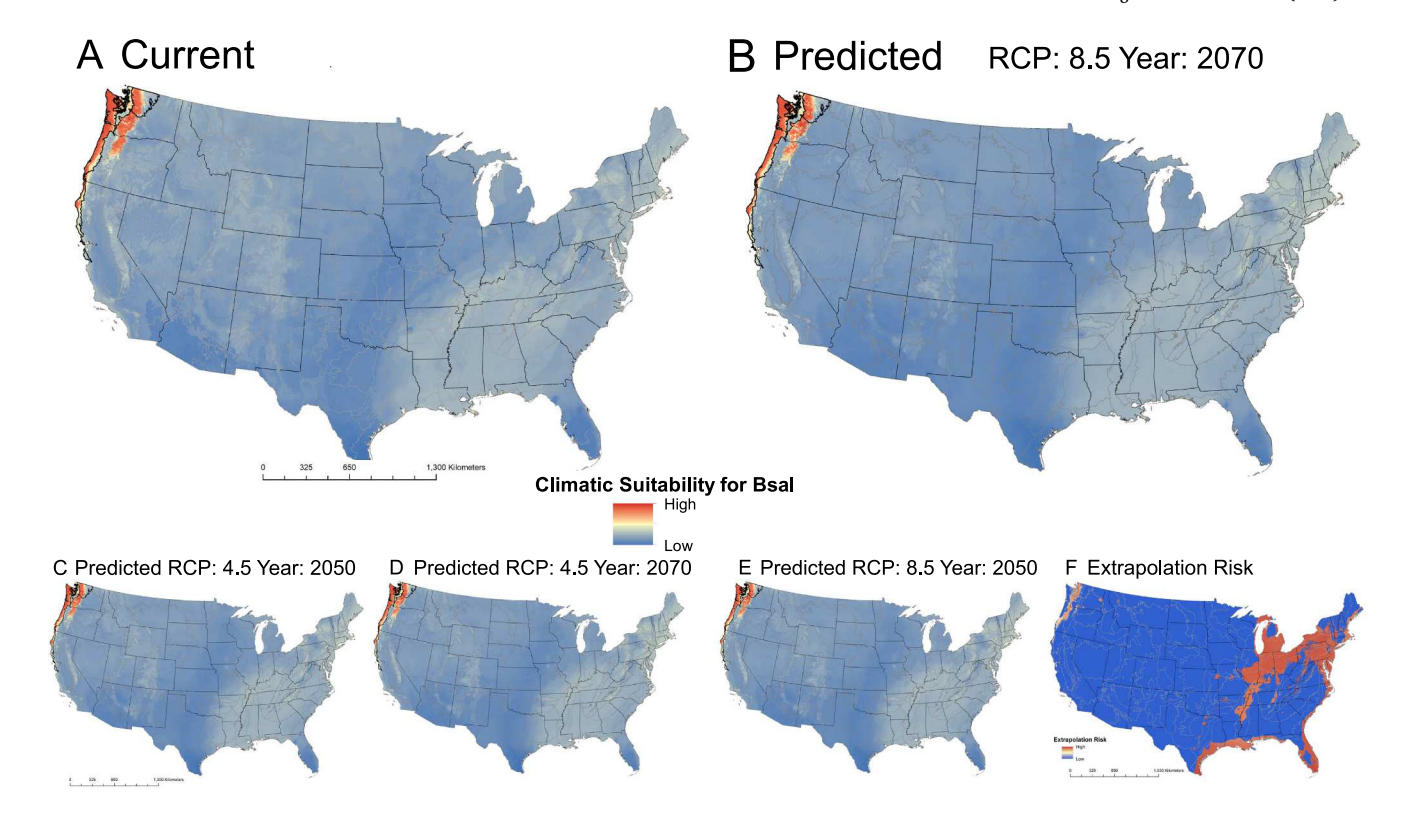


Fig. 2. Climatic suitability models for *Batrachochytrium salamandrivorans* (Bsal). A) Climatic suitability for the Bsal pathogen within the U.S.A. based on current climate data, B) predicted climatic suitability for Bsal within the U.S.A. based on climate projection with RCP 8.5 and year 2070, C) predicted climatic suitability for Bsal within the U.S.A. based on climate projection with RCP 4.5 and year 2050, D) predicted climatic suitability for Bsal within the U.S.A. based on climate projection with RCP 4.5 and year 2070, and E) predicted climatic suitability for Bsal within the U.S.A. based on climate projection with RCP 8.5 and year 2050. For climate models, areas in red display greatest suitability. F) Mobility-oriented parity (MOP) analysis results for extrapolation risk within Bsal models. For the MOP analysis, areas in red indicate areas of high dissimilarity from climates within the native and introduced range of Bsal. Map lines delineate study areas and do not necessarily depict accepted national boundaries. (For interpretation of the references to colour in this figure legend, the reader is referred to the web version of this article.)

both current and the four predicted climate change scenarios.

# 2.4. Estimating risk of Bsal introduction

We estimated Bsal introduction risk into the U.S.A. via human mediated dispersal. To do this, we generated a kernel density map of Flickr photographs within protected lands throughout the U.S.A. We hypothesized that if humans were to unintentionally introduce Bsal into the U.S.A., this would likely occur in a protected area due to the comparably high visitation rates to these habitats and the abundance and diversity of potentially suitable salamander hosts at these locations. Previous work has demonstrated that the number of photographs taken and posted to the social media site Flickr (www.flickr.com) within 38 US national parks was highly correlated with the number of recorded visitors to those parks (Sessions et al., 2016), and has been suggested to be a metric with which to measure park visitation rates (Wood et al., 2013). To generate a kernel density map of photos, we used the R package photosearcher (Fox et al., 2020), which uses the Flickr Application Programming Interface (API) to collect geographic coordinates from posted photos, as well as user information. We used the photo search command

to collect all photos that were taken within protected lands in the U.S.A.

Protected lands were identified using a shapefile of the Protected Areas Dataset of the United States (PADUS; US Geological Survey, Gap Analysis Program 2012), which contains data on the type and extent of protection provided to a landscape. We placed the extent of protection given to a landscape on the following scale of one to four, where one represents landscapes with permanent protection and a management plan that mimics natural disturbance events, two represents an area with permanent protection, but receives management practices that might degrade habitat, three represents permanent protection but has extractive uses, and four represents a landscape that is protected, but lacks data on the protection type. Based on this PADUS database, we defined a protected area as a landscape of one to three on this scale as these areas are most likely to see greatest tourist visitation. Following the methods in Sessions et al. (2016), we limited photos taken within these areas between 01/01/2015 and 12/31/2019. To reduce bias driven by a single user posting many photos from a single day, we subset this database to photos that were unique to a user and a date, which resulted in 32,701 total photos. We transformed these photo coordinates into a kernel density using a combination of the rasterize (raster package;

Table 1
Mean Bsal climatic suitability scores (±standard deviation) for the three most suitable ecoregions in the U.S.A. based on the average of a MaxEnt and RF model.

| Ecoregion      | Current                           | RCP 4.5 year 2050                 | RCP 4.5 year 2070 | RCP 8.5 year 2050                 | RCP 8.5 year 2070 |
|----------------|-----------------------------------|-----------------------------------|-------------------|-----------------------------------|-------------------|
| Coast Range    | $\textbf{74.4} \pm \textbf{20.9}$ | $\textbf{74.4} \pm \textbf{20.9}$ | $74.6 \pm 20.4$   | $\textbf{74.3} \pm \textbf{21.0}$ | $74.1 \pm 21.2$   |
| North Cascades | $56.6 \pm 29.2$                   | $56.8 \pm 30.4$                   | $56.2\pm30.4$     | $55.8 \pm 30.5$                   | $55.1\pm30.8$     |
| Puget Lowlands | $51.6\pm16.3$                     | $49.4\pm16.4$                     | $48.8\pm16.3$     | $48.1\pm16.4$                     | $45.6\pm17.1$     |

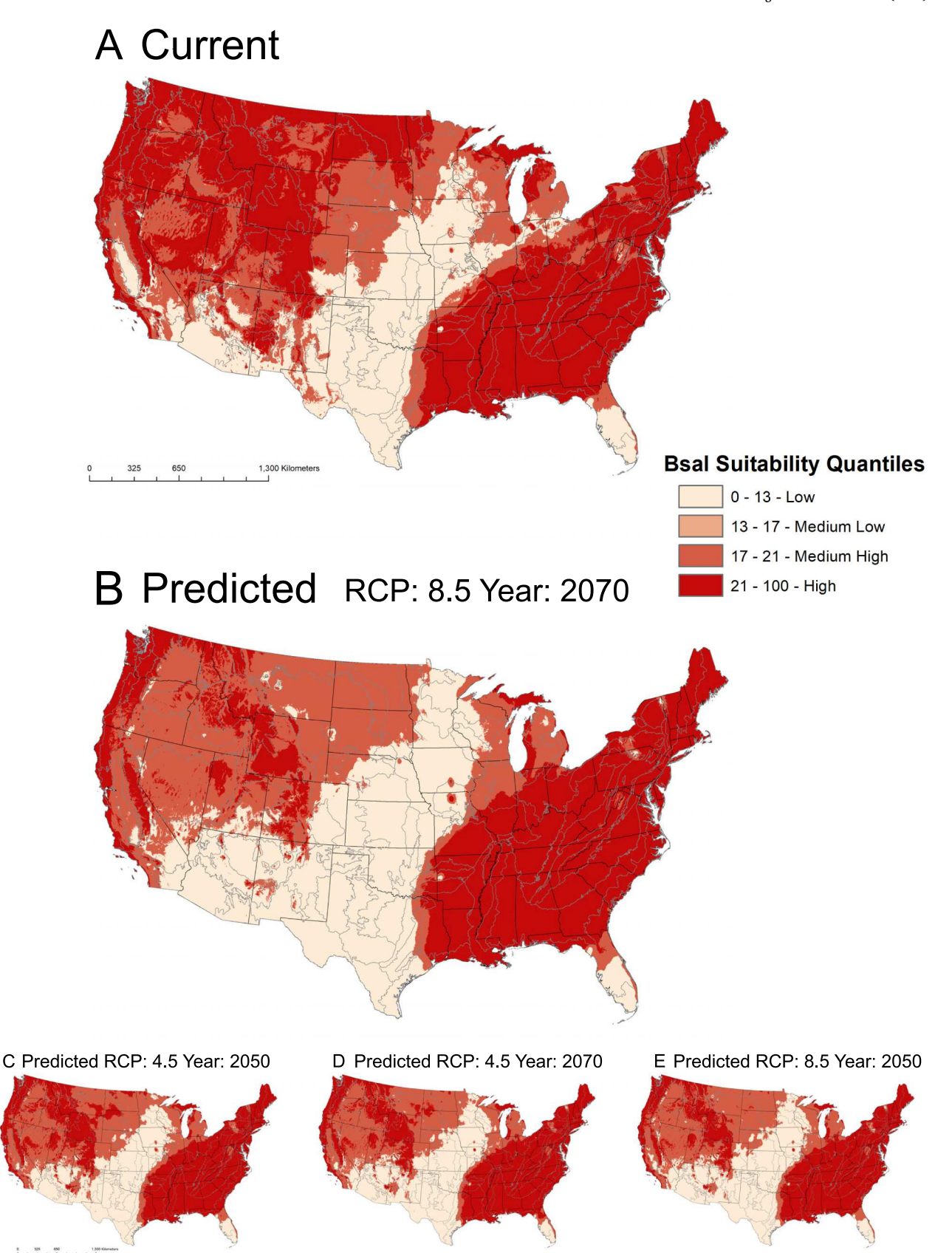


Fig. 3. Climatic suitability model for *Batrachochytrium salamandrivorans* (Bsal) divided into suitability quantiles defined based on the current climate suitability model. A) Climatic suitability for the Bsal pathogen within the U.S.A. based on current climate data, B) predicted climatic suitability for Bsal within the U.S.A. based on climate projection with RCP 8.5 and year 2070, C) predicted climatic suitability for Bsal within the U.S.A. based on climate projection with RCP 4.5 and year 2070, and E) predicted climatic suitability for Bsal within the U.S.A. based on climate projection with RCP 4.5 and year 2070, and E) predicted climatic suitability for Bsal within the U.S.A. based on climate projection with RCP 8.5 and year 2050. Map lines delineate study areas and do not necessarily depict accepted national boundaries.

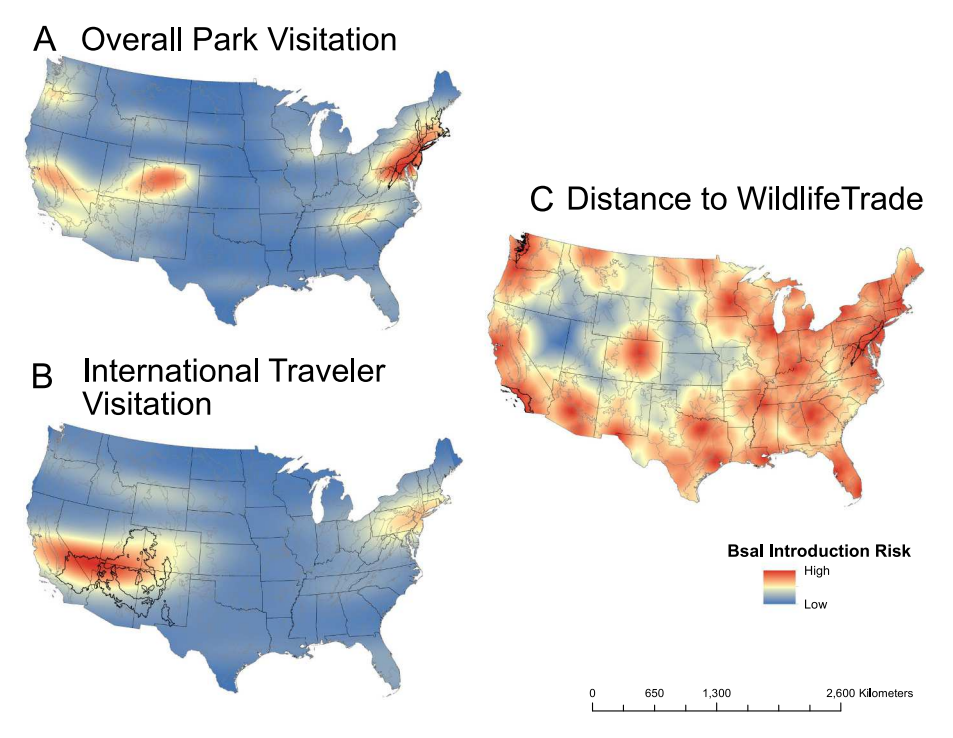


Fig. 4. Risk of introduction of Batrachochytrium salamandrivorans (Bsal) into the U.S.A. represented by, A) overall US park visitation rates as determined by Flickr photograph density, B) US park international visitation rates as determined by Flickr photograph density, and C) Euclidean distance to the wildlife trade, including pet stores and reptile shows. Areas in red represent areas with greater risk of Bsal introduction either due to proximity to high park usage (A and B) or close proximity to the wildlife trade (C). Map lines delineate study areas and do not necessarily depict accepted national boundaries. (For interpretation of the references to colour in this figure legend, the reader is referred to the web version of this article.)

Hijmans et al., 2013) and *kde2d* command (*MASS* package; Ripley et al., 2013) to generate a raster showing protected area visitation rates. As Bsal has not yet been detected in the U.S.A., we generated a second kernel density map of photographs taken by international photographers to weight protected areas visited by international travelers more heavily. We used the *user\_info* command (*photosearcher* package; Fox et al., 2020) to identify unique photographers (5757) that took pictures in protected areas between 01/01/2015 and 12/31/2019. Using a combination of user provided home country and current city, we removed all users that were from the U.S.A., resulting in 902 unique individual international photographers. We then generated a second kernel density map of photographs taken by these international photographers to represent international park visitation rates.

A second hypothesized route of Bsal transmission into the U.S.A. is through a spillover event from the wildlife/pet-trade (Richgels et al., 2016). To determine landscape distance to pet trade vendors, we used the 2019 U.S.A. census data to identify U.S.A. zip codes where pet stores (code: North American Industry Classification System; 45391) were located. Additionally, we conducted a Google search to identify the location of major exotic pet shows across the U.S.A. In total, we generated a database of the locations of 94 exotic pet shows planned for 2022. For the pet store location and reptile show location databases, we generated a raster layer that represented the Euclidean distance of a raster cell to the nearest pet store/reptile show. We assumed that if Bsal was introduced into the U.S.A. through the wildlife trade, the risk will have a negative relationship with the distance to a trade event. These

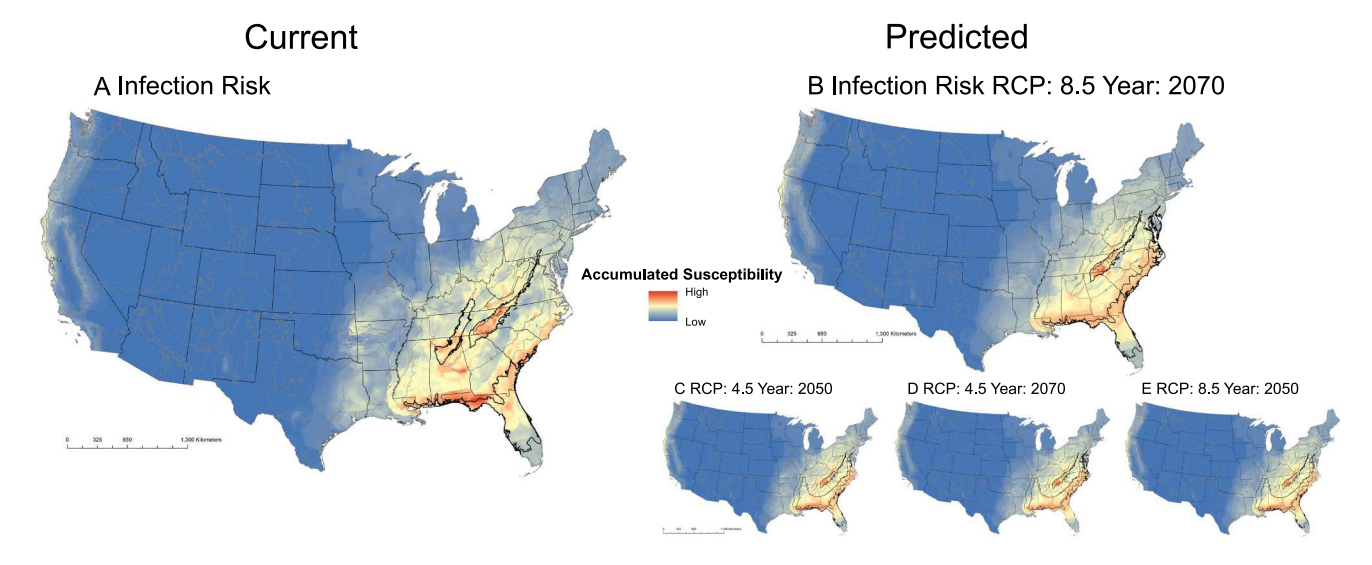


Fig. 5. Current and predicted accumulated *Batrachochytrium salamandrivorans* infection risk. (A) Current infection risk to salamander populations across the U.S.A. based on current climate models, (B) predicted infection risk based on climate models with RCP 8.5 at year 2070, (C) predicted infection risk based on climate models with RCP 4.5 at year 2050, (D) predicted infection risk based on climate models with RCP 4.5 at year 2050. Map lines delineate study areas and do not necessarily depict accepted national boundaries.

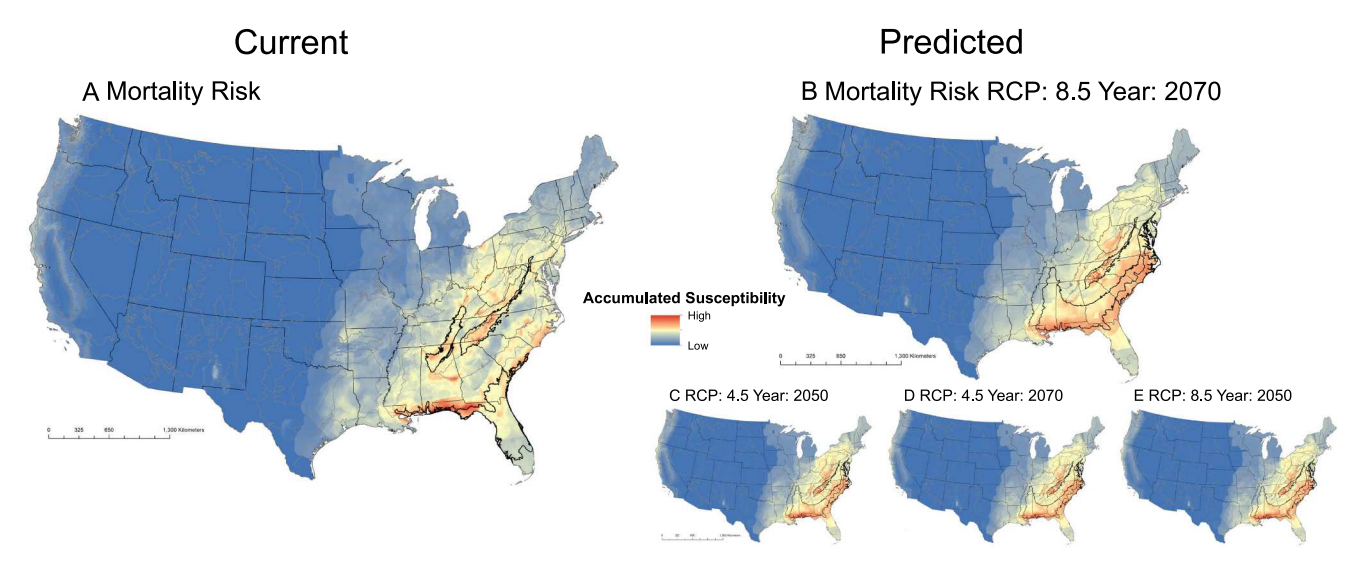


Fig. 6. Current and predicted accumulated *Batrachochytrium salamandrivorans* mortality risk. (A) Current mortality risk to salamander populations across the U.S.A. based on current climate models, (B) predicted mortality risk based on climate models with RCP 8.5 at year 2070, (C) predicted mortality risk based on climate models with RCP 4.5 at year 2070, and (E) predicted mortality risk based on climate models with RCP 8.5 at year 2070, and (E) predicted mortality risk based on climate models with RCP 8.5 at year 2050. Map lines delineate study areas and do not necessarily depict accepted national boundaries.

two raster layers were averaged into a single raster of distance to wildlife trade and represented the risk associated with potential Bsal spillover from the wildlife trade (Richgels et al., 2016).

After formation of all rasters, we reclassified each to a scale of 0–100, with 100 representing greatest risk. For distance to wildlife trade, after rescaling the data on a 0–100 scale, we subtracted the layer from 100 to allow a value of 100 to represent the greatest risk. The Flickr-generated park visitation rasters were resampled using bilinear interpolation to match the resolution and extent of other layers.

# 2.5. Overall invasion risk

To generate an overall risk prediction for the invasion of Bsal into the U.S.A., we evaluated risk based on three components, including introduction risk, consequences of Bsal introduction, and Bsal suitability. We calculated the average value for the introduction of Bsal (raster layers: distance to wildlife trade, international park visitation, and park visitation) and the average for consequences of Bsal introduction (raster layers: mortality and infection). We added these two mean values to the current and projected Bsal climatic suitability, and then reclassified these raster layers on a scale of 0–100, with 100 representing greatest risk of Bsal emergence. We summarized all metrics by EPA Level III ecoregions, which represent effective conservation units (Olson and Dinerstein, 1998) and provide a framework for relating impacts of landuse on biodiversity patterns (Gallant et al., 2004).

# 3. Results

# 3.1. Estimating Bsal climatic suitability and shifts due to climate change

Our models for Bsal climatic suitability had good fit (MaxEnt AUC:  $0.81\pm0.07$ , TSS:  $0.53\pm0.1$ ; RF AUC:  $0.75\pm0.06$ , TSS:  $0.44\pm0.08$ ). The MOP analysis identified areas in the Northeastern and Southeastern coasts as well as areas in the Northwestern U.S.A. as areas of high extrapolation risk (Fig. 2f), suggesting that the interpretation of climatic suitability of Bsal within those areas should be done with caution. Model selection via AICc identified the model that included the regularization parameter set to 2 and hinge set as feature class as the model that best explained the data. Under current climatic conditions, climatic suitability (on a scale of 0–100, with 100 representing greatest suitability) for Bsal was greatest on the west coast of the U.S.A., with the Coast

Range (mean: 74.4  $\pm$  21.1; Fig. 2a; Table 1), North Cascades (mean: 56.6  $\pm$  29.2; Fig. 2a; Table 1), and the Puget Lowland (mean: 51.6  $\pm$  16.3; Fig. 2a; Table 1) ecoregions having greatest suitability.

Under climatic conditions predicted by the most extreme model (RCP 8.5 at year 2070), average Bsal suitability was predicted as greatest in the Coast Range (mean:  $74.1 \pm 21.2$ ; Fig. 2b; Table 1), North Cascades (mean:  $55.1 \pm 30.8$ ; Fig. 2b; Table 1), and the Puget Lowland (mean:  $45.6 \pm 17.1$ ; Fig. 2b; Table 1) ecoregions. Across all models, 35 ecoregions (41 %) had at least one climate model predicting an increase in average climatic suitability for Bsal. Of these 35 ecoregions, 29 increased in suitability for all models, two increased for all models except for RCP 8.5 at year 2070, three increased for all models with RCP 4.5, and one ecoregion increased only for the RCP 4.5 at year 2070.

At a broader scale, the two greatest suitability quantiles, High and Medium High, lost the greatest area across models due to predicted climate change (Fig. 3). Both High and Medium High quantiles went from 27 % and 26 % respectively of the total area, to 24 % (High) and 12 % (Medium High) of the total area (Fig. 3), representing a large loss of potentially climatically suitable area for Bsal. All results are reported in Supplemental File 2 tables S2.5–2.9.

# 3.2. Estimating human-mediated risk of Bsal introduction

Overall, protected area visitation as determined by Flickr photograph density was greatest in the Northern Piedmont (mean: 89.4  $\pm$ 12.0, on a scale of 0-100, with 100 representing highest visitation), Atlantic Coastal Pine Barrens (mean:  $79.7 \pm 11.3$ ; Fig. 4a), and the Northeastern Coastal Zone (mean:  $65.4 \pm 12.6$ ; Fig. 4a) ecoregions. Secondary hotspots included the Ridge and Valley (54.6  $\pm$  24), Southern Rockies (51.4  $\pm$  24.0), Sierra Nevada (51.5  $\pm$  16.3), and Blue Ridge (50.3  $\pm$  13.5) ecoregions. International visitation rates as determined by Flickr photograph density was greatest in the Mojave Basin and Range (mean: 75.5  $\pm$  19.9; Fig. 4b), Colorado Plateaus (mean: 63.9  $\pm$  17.8; Fig. 4b), and Arizona/New Mexico Plateau (mean: 59.3  $\pm$  20.3; Fig. 4b) ecoregions. A secondary hotspot of international visitation rates was found in the Atlantic Coastal Pine Barrens (56.0  $\pm$  5.6; Fig. 4b), and Northern Piedmont (52.0  $\pm$  11; Fig. 4b). Distance to wildlife trade was smallest (highest introduction risk) in the Northern Piedmont (mean: 7.3  $\pm$  3.9; Fig. 4c), Puget Lowland (mean: 7.8  $\pm$  3.7; Fig. 4c), and Southern California/Northern Baja Coast (mean: 8.0  $\pm$  4.3; Fig. 4c) ecoregions.

A) Greatest mean accumulated infection rates (±standard deviation) for the three ecoregions that scored greatest for this metric under each current and predicted climate model. B) Greatest mean accumulated mortality

| Current                                |                | RCP 4.5 year 2050                   |               | RCP 4.5 year 2070                   |                          | RCP 8.5 year 2050                   |               | RCP 8.5 year 2070                   |                 |
|--|----------------|-------------------------------------|---------------|-------------------------------------|--------------------------|-------------------------------------|---------------|-------------------------------------|-----------------|
| A) Infection<br>Blue Ridge             | $60.7\pm11.5$  | Blue Ridge                          | $61.1\pm12.3$ | Blue Ridge                          | $60.7\pm12.8$ Blue Ridge | Blue Ridge                          | $60.4\pm12.9$ | Blue Ridge                          | $59.9 \pm 13.2$ |
| Southwestern                           | $53.7 \pm 9.8$ | Southeastern Plains                 | $55.1\pm10.7$ | Southeastern Plains                 | $54.3 \pm 10.5$          | Southeastern Plains                 | $54.3\pm10.7$ | Southern Coastal Plain              | $54.2 \pm 13.0$ |
| Appalachians<br>Southern Coastal Plain | $53.6\pm15.1$  | Southern Coastal Plain              | $54.2\pm13.0$ | Middle Atlantic Coastal Plain       | $53.9\pm15.5$            | Southern Coastal Plain              | $54.0\pm12.8$ | Middle Atlantic Coastal Plain       | $53.9 \pm 15.5$ |
| B) Mortality                           |                |                                     |               |                                     |                          |                                     |               |                                     |                 |
| Blue Ridge                             | $58.8 \pm 8.3$ | Blue Ridge                          | $64.7\pm11.1$ | Blue Ridge                          | $64.3 \pm 11.6$          | Blue Ridge                          | $63.6\pm11.4$ | Blue Ridge                          | $61.9 \pm 11.6$ |
| Southwestern                           | $54.6 \pm 7.7$ | Middle Atlantic Coastal Plain       | $55.1\pm10.7$ | Middle Atlantic Coastal Plain       | $61.4\pm12.8$            | Middle Atlantic Coastal Plain       | $60.8\pm12.6$ | Middle Atlantic Coastal Plain       | $61.2 \pm 13.0$ |
| Appalachians                           |                |                                     |               |                                     |                          |                                     |               |                                     |                 |
| Southern Coastal Plain                 | $50.0\pm14.0$  | $50.0 \pm 14.0$ Southeastern Plains | $54.2\pm13.0$ | $54.2 \pm 13.0$ Southeastern Plains | $59.4\pm11.6$            | $59.4 \pm 11.6$ Southeastern Plains | $59.7\pm11.7$ | $59.7 \pm 11.7$ Southeastern Plains | $58.6\pm10.9$   |

### 3.3. Estimating consequences of introduction

Under current climatic conditions, accumulated infection risk (on a scale of 0–100, with 100 representing greatest risk) was greatest on the eastern coast of the U.S.A., with greatest risk in the Blue Ridge (mean:  $60.7\pm11.5;$  Fig. 5a), Southwestern Appalachians (mean:  $53.7\pm9.8;$  Fig. 5a), and Southern Coastal Plains (mean:  $53.6\pm15.1;$  Fig. 5a) ecoregions. Under current climatic conditions, accumulated mortality risk was also greatest in this region, with the Blue Ridge (mean:  $58.8\pm8.3;$  Fig. 6a), Southwestern Appalachians (mean:  $54.6\pm7.7$  Fig. 6a), and Southern Coastal Plain (mean:  $50.0\pm14.0$  Fig. 6a) ecoregions having greatest risk.

Under climatic conditions predicted by the most extreme model (RCP 8.5 and at the year 2070), accumulated infection risk was greatest in the Blue Ridge (mean:  $59.9 \pm 13.2$ ; Fig. 5b; Table 2a), Southern Coastal Plain (mean:  $54.2 \pm 13.0$ ; Fig. 5b; Table 2a), and Middle Atlantic Coastal Plain (mean:  $53.9 \pm 15.5$ ; Fig. 5b; Table 2a) ecoregions. Under climatic conditions predicted by models with RCP 8.5 and at the year 2070, accumulated mortality risk followed the same pattern as infection risk and was greatest in the Blue Ridge (mean:  $61.9 \pm 11.6$ ; Fig. 6b; Table 2b), Middle Atlantic Coastal Plain (mean:  $61.2 \pm 13.0$ ; Fig. 6b; Table 2b), and Southeastern Plains (mean:  $58.6 \pm 10.9$ ; Fig. 6b; Table 2b) ecoregions.

# 3.4. Overall risk of Bsal invasion (all metrics combined)

The Bsal invasion risk under current climatic conditions was greatest in the Blue Ridge (Risk value:  $68.8 \pm 8.4$ ; Fig. 7a), Coast Range (Risk value: 67.8  $\pm$  10.3; Fig. 7a), Atlantic Coastal Pine Barrens (Risk value: 65.4  $\pm$  4.6; Fig. 7a), and Northern Piedmont (Risk value: 66.7  $\pm$  6.5; Fig. 7a) ecoregions. For the Blue Ridge, the predicted high risk was driven by a high consequence of introduction, with high accumulated infection (mean:  $60.6 \pm 11.5$ ), as well as high accumulated mortality (mean:  $58.8 \pm 8.3$ ). For the Coast Range, the high risk was driven by Bsal climatic suitability (mean: 74.4  $\pm$  21.1). For the Atlantic Coastal Pine Barrens, the high risk was driven by high introduction risks, specifically a low distance to the wildlife trade (mean:  $8.0 \pm 3.7$ ), as well as high overall protected area visitation (mean: 79.7  $\pm$  11.3), and high international protected area visitation (mean: 56.0  $\pm$  5.6). For the Northern Piedmont ecoregion, the high risk was caused by the high introduction risks, specifically high protected area visitation (mean: 89.4  $\pm$  12.0), high international park visitation (mean: 52.0  $\pm$  11.0), and low distance to wildlife trade (mean: 7.3  $\pm$  3.9). Lastly, the Northern Piedmont ecoregion had high accumulated mortality risk (mean:  $48.3 \pm 5.8$ ).

Under climatic conditions predicted by all models (RCP 4.5 at year 2050 and 2070, and RCP 8.5 at year 2050 and 2070), overall risk for Bsal introduction was greatest in the Coast Range (mean risk range: 64.4  $\pm$ 10.0–66.8  $\pm$  10.3), Blue Ridge (mean risk range: 63.2  $\pm$  8.6–66.2  $\pm$ 8.5), Northern Piedmont (mean risk range:  $60.3 \pm 3.6$ – $61.7 \pm 3.4$ ), and Atlantic Coastal Pine Barrens (mean risk range:  $59.8 \pm 3.9 - 61.7 \pm 3.8$ ) ecoregions. The high overall risk for the Coast Range was driven by high climatic suitability for Bsal (mean suitability range: 74.1  $\pm$  21.2–74.6  $\pm$ 20.4). For the Blue Ridge ecoregion, the overall high risk was attributed to high values for both mean accumulated infection (mean infection range: 59.9  $\pm$  13.2-61.1  $\pm$  12.3) and accumulated mortality (mean mortality range:  $61.9 \pm 11.6$ – $64.3 \pm 11.6$ ). For the Northern Piedmont, the overall high risk was driven by high introduction risks, specifically high overall protected area visitation (mean visitation:  $84.4 \pm 12.0$ ), high international protected area visitation (mean visitation: 52.0  $\pm$ 11.0), and low distance to wildlife trade (mean distance:  $7.3 \pm 4.0$ ). Lastly, for the Atlantic Coastal Pine Barrens, the high overall risk was driven by a combination of protected area visitation both overall (mean visitation: 79.7  $\pm$  11.3), as well as protected area visitation by international visitors (mean visitation: 56.0  $\pm$  5.6), and relatively high climatic suitability for Bsal (mean suitability range: 32.0  $\pm$  9.1–33.4  $\pm$ 

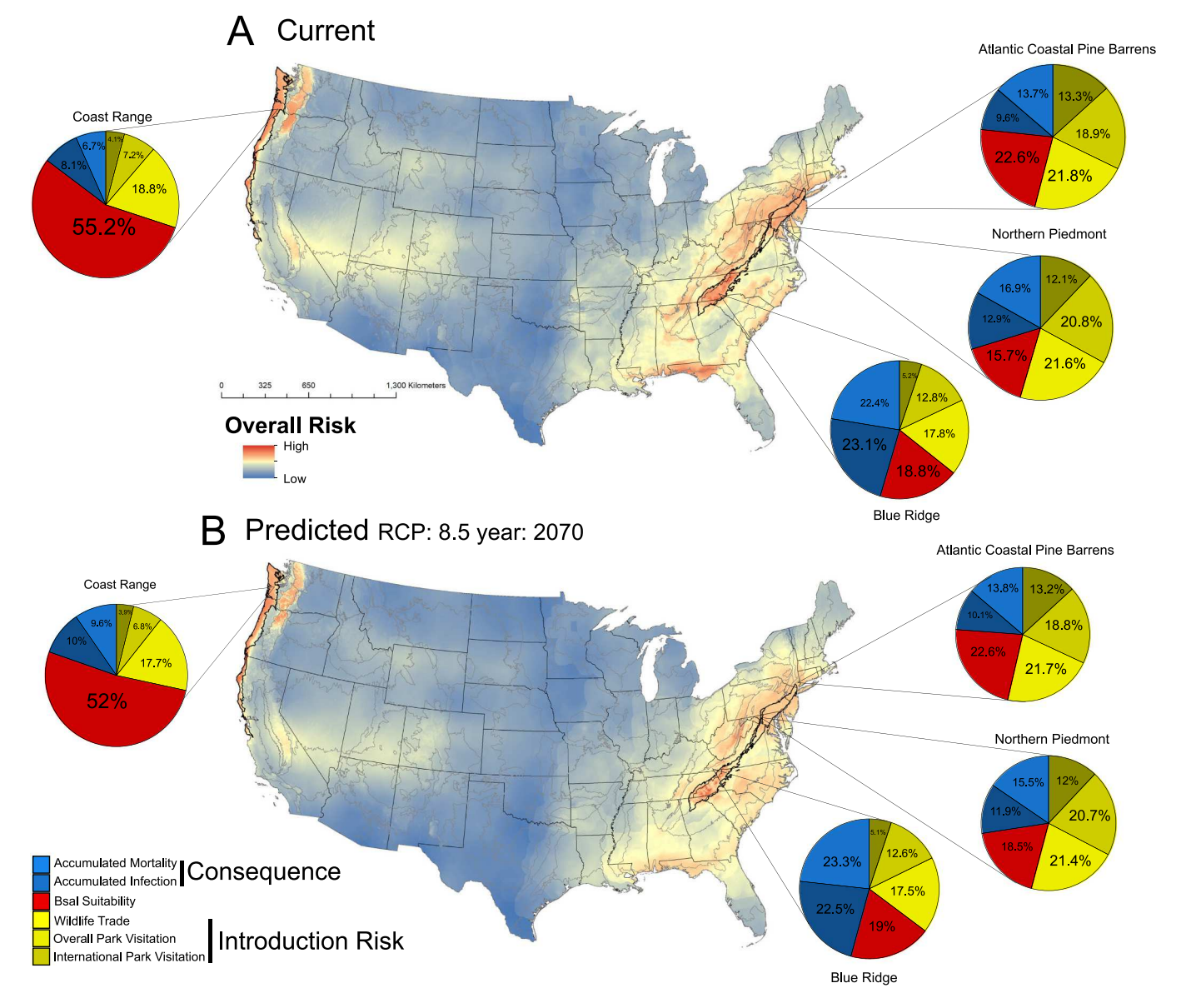


Fig. 7. Overall risk of *Batrachochytrium salamandrivorans* (Bsal) emergence in the U.S.A based on A) current climatic conditions and B) predicted climatic conditions under the RCP 8.5 scenario and at the year 2070. The overall risk model takes into account: Bsal climatic suitability, infection and mortality risks, distance to pet trade, and protected area use based on total and international visitation rates. Landscapes in red are at greatest risk of Bsal emergence. Pie charts show the percent contribution each metric has in the risk analysis for the top four most at risk ecoregions determined from the current climate analysis. Map lines delineate study areas and do not necessarily depict accepted national boundaries. (For interpretation of the references to colour in this figure legend, the reader is referred to the web version of this article.)

9.6). Overall, under predicted climate models, risk values were lower, driven mostly by the reduction in Bsal climatic suitability (Fig. 7b; Table 3).

### 4. Discussion

Due to high salamander species richness in the U.S.A., understanding and predicting how Bsal may emerge is a conservation priority (Gray et al., 2015). Overall, our analysis suggests that under both current and predicted climatic conditions, the Coast Range, Blue Ridge, Northern Piedmont, and Atlantic Coastal Pine Barrens ecoregions are at greatest risk for Bsal emergence. In general, the drivers of high risk in our models were the accumulated infection and mortality values, which we referred to as the consequences of introduction. The most at-risk ecoregions had the greatest number of susceptible hosts. This pattern was also observed in previously published risk predictions, with the southeastern and

northwestern U.S.A. representing areas of high risk for Bsal emergence (Richgels et al., 2016; Yap et al., 2015).

In general, our model suggests that patterns of accumulated infection and mortality follow patterns of salamander richness. This provides evidence in support of previous assumptions that Bsal emergence risk scales with local salamander richness (Richgels et al., 2016; Yap et al., 2015). Furthermore, models of changes in suitability due to climate change support previous patterns of shifting climatic suitability, specifically towards higher elevations, as well as higher latitudes (Lyons and Kozak, 2020). As a result of this shift in climatic conditions, there is a predicted shift in both accumulated infection and accumulated mortality towards the coasts and towards greater elevations in landscapes that are currently climatically suitable for the Bsal pathogen. It is important to note that our modeling of Bsal susceptibility (infection and mortality) is informative only for the risk of pathogen introduction and should be used with caution when inferring spread of Bsal within

Biological Conservation 284 (2023) 110181

Table 3
Mean values for each of the factors that contribute to overall Bsal emergence risk in the U.S.A. for current climate models (A), and predicted models based on RCP 4.5 at year 2050 (B), RCP 4.5 at year 2070 (C), RCP 8.5 at year 2050 (D), and RCP 8.5 at year 2070 (E). Across models, the Coast Range and the Blue Ridge ecoregions are at greatest risk.

| Ecoregion                     | Mean current Bsal suitability scores $(\pm SD)$ | Mean accumulated infection ( $\pm SD$ ) | Mean accumulated mortality ( $\pm SD$ ) | Mean distance to wildlife trade ( $\pm SD$ ) | Mean Protected Area use $(\pm SD)$ | Mean Protected Area use by international visitors ( $\pm SD$ ) | Overall risk $(\pm SD)$ |
|-------------------------------|---|---|---|--|------------------------------------|--|-------------------------|
| A) Current                    |   |   |   |  |                                    |  |                         |
| Atlantic Coastal Pine Barrens | $31.8 \pm 9.9$                                  | $27.1 \pm 6.5$                          | $38.5 \pm 9.6$                          | $8.0\pm3.7$                                  | $79.7 \pm 11.3$                    | $56.0 \pm 5.6$   | $65.4 \pm 4.6$          |
| Blue Ridge                    | $24.7 \pm 3.2$                                  | $60.7\pm11.5$                           | $58.8 \pm 8.3$                          | $30.0\pm11.7$                                | $50.3\pm13.5$                      | $20.4 \pm 7.1$   | $68.8 \pm 8.4$          |
| Coast Range                   | $\textbf{74.4} \pm \textbf{21.1}$               | $21.7\pm10.6$                           | $17.9 \pm 7.2$                          | $24.2\pm11.5$                                | $29.1\pm12.4$                      | $16.6\pm11.1$  | $67.8\pm10.3$           |
| Northern Piedmont             | $22.5\pm3.6$                                    | $36.9 \pm 4.5$                          | $48.3\pm5.8$                            | $7.3\pm3.9$                                  | $89.4\pm12.0$                      | $52.0\pm11.0$  | $66.7 \pm 6.5$          |
| B) RCP 4.5 at 2050            |   |   |   |  |                                    |  |                         |
| Atlantic Coastal Pine Barrens | $32.6 \pm 9.9$                                  | $27.7 \pm 5.8$                          | $39.7 \pm 7.8$                          | $8.0\pm3.7$                                  | $79.7 \pm 11.3$                    | $56.0 \pm 5.6$   | $61.7 \pm 3.8$          |
| Blue Ridge                    | $25.3 \pm 2.8$                                  | $61.1\pm12.3$                           | $64.7\pm11.2$                           | $30.1\pm11.7$                                | $50.3\pm13.5$                      | $20.4 \pm 7.1$   | $66.2 \pm 8.5$          |
| Coast Range                   | $74.4\pm20.8$                                   | $27.0\pm10.8$                           | $25.4 \pm 7.8$                          | $24.2\pm11.5$                                | $29.1\pm12.4$                      | $16.6\pm11.1$  | $66.8\pm10.3$           |
| Northern Piedmont             | $24.6\pm2.6$                                    | $34.3 \pm 5.8$                          | $46\pm4.2$                              | $7.3\pm3.9$                                  | $89.4 \pm 12.0$                    | $52.0\pm11.0$  | $61.7\pm3.4$            |
| C) RCP 4.5 at 2070            |   |   |   |  |                                    |  |                         |
| Atlantic Coastal Pine Barrens | $33.4 \pm 9.6$                                  | $28.1 \pm 6.0$                          | $40.0\pm7.9$                            | $8.0 \pm 3.7$                                | $79.7 \pm 11.3$                    | $56.0 \pm 5.6$   | $59.8 \pm 3.9$          |
| Blue Ridge                    | $25.3 \pm 2.9$                                  | $60.7 \pm 12.8$                         | $64.3 \pm 11.6$                         | $30.1\pm11.7$                                | $50.3\pm13.5$                      | $20.4 \pm 7.1$   | $63.2 \pm 8.6$          |
| Coast Range                   | $74.6\pm20.4$                                   | $27.3 \pm 10.4$                         | $26.1 \pm 7.6$                          | $24.2 \pm 11.5$                              | $29.1\pm12.4$                      | $16.6\pm11.1$  | $64.4\pm10.0$           |
| Northern Piedmont             | $26.0\pm3.0$                                    | $34.9 \pm 6.0$                          | $46.9 \pm 4.5$                          | $7.3\pm3.9$                                  | $89.4\pm12.0$                      | $52.0\pm11.0$  | $60.3\pm3.6$            |
| D) RCP 8.5 at 2050            |   |   |   |  |                                    |  |                         |
| Atlantic Coastal Pine Barrens | $32.2 \pm 9.5$                                  | $28.2 \pm 6.0$                          | $40.1 \pm 8.0$                          | $8.0 \pm 3.7$                                | $79.7 \pm 11.3$                    | $56.0 \pm 5.6$   | $60.4 \pm 4.0$          |
| Blue Ridge                    | $24.9 \pm 2.7$                                  | $60.4\pm12.9$                           | $63.6 \pm 11.4$                         | $30.1\pm11.7$                                | $50.3\pm13.5$                      | $20.4 \pm 7.1$   | $63.9 \pm 8.6$          |
| Coast Range                   | $74.3 \pm 21.0$                                 | $27.4 \pm 10.3$                         | $26.3 \pm 7.6$                          | $24.2\pm11.5$                                | $29.1\pm12.4$                      | $16.6\pm11.1$  | $65.6\pm10.0$           |
| Northern Piedmont             | $25.1\pm2.5$                                    | $34.3 \pm 5.7$                          | $46.0\pm4.5$                            | $7.3\pm3.9$                                  | $89.4\pm12.0$                      | $52.0\pm11.0$  | $60.6\pm3.3$            |
| E) RCP 8.5 at 2070            |   |   |   |  |                                    |  |                         |
| Atlantic Coastal Pine Barrens | $32.0 \pm 9.1$                                  | $28.5 \pm 6.4$                          | $38.9 \pm 8.0$                          | $8.0\pm3.7$                                  | $79.7 \pm 11.3$                    | $56.0 \pm 5.6$   | $60.3 \pm 4.2$          |
| Blue Ridge                    | $25.3\pm2.5$                                    | $59.9 \pm 13.2$                         | $61.9 \pm 11.6$                         | $30.1\pm11.7$                                | $50.3\pm13.5$                      | $20.4 \pm 7.1$   | $63.8 \pm 8.6$          |
| Coast Range                   | $74.1 \pm 21.2$                                 | $28.5 \pm 9.9$                          | $27.5 \pm 7.2$                          | $24.2\pm11.5$                                | $29.1\pm12.4$                      | $16.6\pm11.1$  | $66.5\pm11.0$           |
| Northern Piedmont             | $26.6 \pm 2.0$                                  | $34.5 \pm 5.6$                          | $44.7 \pm 5.0$                          | $7.3 \pm 3.9$                                | $89.4 \pm 12.0$                    | $52.0\pm11.0$  | $61.5 \pm 3.2$          |

salamander assemblages. Understanding how amphibian diversity and abundance interact to influence pathogen dynamics is not well understood (Rohr et al., 2020); however, previous studies on amphibian assemblages have shown both pathogen dilution (negative relationship between diversity and pathogen abundance; Venesky et al., 2014), and amplification (positive relationship; Tornabene et al., 2018) within amphibian host-pathogen systems.

Our models predict that the greatest climatic suitability for Bsal, both currently and under projected climate change, is predicted in the northwestern U.S.A. Our current climate model agrees with other suitability models produced by Yap et al. (2015), Richgels et al. (2016), and Moubarak et al. (2022). Differences in climatic suitability across these risk models are likely attributed to differences in modeling algorithms. For example, Richgels et al. (2016) used a mechanistic approach based on a thermal maximum temperature for Bsal (25 °C) to identify climatically suitable landscapes. This mechanistic approach may overpredict suitable climate (Buckley et al., 2010), as the assumed reliance exclusively on temperature is likely an oversimplification of physiological and ecological requirements. On the other hand, our model, like Yap et al. (2015), used a correlative approach, which has been suggested to under-predict invasive species ranges (Tingley et al., 2014). While our model and the Yap et al. model are similar, Yap et al. (2015) found a second highly suitable area further south along the eastern coast of the U.S.A., which was only moderately suitable in our model. This difference in suitability may be due to the differences in the species occurrence points, along with our incorporation of the RF modeling approach. Yap et al. (2015) used occurrences of salamanders that are known to carry Bsal in their native range in Asia, whereas our model used points of Bsal positive salamanders sampled in both Asia and Europe.

When comparing the suitability scores associated with the highest quantiles under current and predicted climate models, in general there is a reduction in highly suitable climatic conditions for Bsal. It is likely that this reduction in highly suitable climatic conditions is due to predicted increased temperatures. Previous work has suggested that Bsal has a thermal maximum temperature of 25 °C (Martel et al., 2013). In addition, our models show that suitable climate shifts towards higher elevations and latitudes, similar to what has been predicted for Bd (Xie et al., 2016). This shift is especially apparent in the Rocky Mountain region, where only the greatest elevations maintain high suitability. It is important to note that the grain of our study was based on our raster dataset, which had a resolution of 30 s (approximately 1 km<sup>2</sup>). Therefore, at this scale we cannot assess the role of microenvironments in climatic suitability, likely resulting in an under-prediction of both risk and suitable habitat across the U.S.A. Additionally, our model of climatic suitability for Bsal was based on 77 occurrence points, and while it has been shown that MaxEnt can generate accurate predications based on as few as 30 points (Wisz et al., 2008), increasing the sampling effort for Bsal, and ultimately occurrence points, within its native and introduced range will help refine future predictions of climatic suitability.

Provided that the U.S.A. leads the world in amphibian imports (Can et al., 2019), it is likely that Bsal emergence is only a matter of time, considering practices that promote international clean trade of wildlife are not encouraged or required in the U.S.A. (Richgels et al., 2016; Yap et al., 2015). Previous work has suggested that the risk of Bsal emergence due to spillover will scale with the Euclidean distance from the pet trade (Richgels et al., 2016); however, this may be an oversimplification of this risk. The online pet trade has increased in popularity (Siriwat and Nijman, 2020) and obscures the relationship between wildlife trade locations and spillover risk. While previous risk models have emphasized the pet trade as a major introduction route for Bsal, multiple wildlife pathogens have likely emerged through fomite-mediated dispersal, i.e., Pseudogymnoascus destructans (Blehert et al., 2009) and Batrachochytrium dendrobatidis (Walker et al., 2008). Here, we used protected area visitation rates as a metric of risk for fomite-mediated pathogen dispersal and encourage others to consider this approach in future risk analyses. One of the major hotspots identified in our analysis contains the epicenter for *P. destructans* spread in the U.S.A. (Blehert et al., 2009), providing additional support that introduction of novel pathogens via fomite-mediated dispersal to protected areas with high visitation rates is a real threat.

Across climate models, we found that the greatest risk of Bsal emergence in the U.S.A. is predicted in the Southeast and Northwest, following patterns of salamander species susceptibilities. Across climate change models, there is a general lack of change in overall risk at the ecoregion level, however, there is a general reduction in predicted climatic suitability for Bsal. Our models add to the growing literature predicting risk of Bsal emergence in the U.S.A. via incorporation of variation in species susceptibilities paired with the additional influence of climate change and human-mediated introductions. Conservation efforts should focus on preventing the spread of Bsal in the U.S.A. and North America, as preventative measures are more cost effective than removal or mitigation efforts (Karesh et al., 2005). Additionally, efforts should include enhanced surveillance and monitoring, especially in the pet trade and areas with high salamander diversity. Future work should aim to understand the role of microhabitats for affecting Bsal environmental suitability and persistence and incorporate estimates into risk assessments, as well as continued evaluations of species susceptibilities to the Bsal pathogen.

### CRediT authorship contribution statement

Matthew Grisnik: Conceptualization, Data curation, Formal analysis, Investigation, Methodology, Visualization, Writing – original draft, Writing – review & editing. Matthew J. Gray: Data curation, Funding acquisition, Writing – original draft, Writing – review & editing. Jonah Piovia-Scott: Data curation, Funding acquisition, Writing – original draft, Writing – review & editing. Edward Davis Carter: Data curation, Writing – original draft, Writing – review & editing. William B. Sutton: Conceptualization, Funding acquisition, Investigation, Methodology, Project administration, Resources, Supervision, Writing – original draft, Writing – review & editing.

# **Declaration of competing interest**

The authors declare no conflict of interests.

# Data availability

All data used are taken from published sources and cited in text, all code used to generate figures is included in the Supplemental File.

### Acknowledgements

Funding and support for this research project was provided by the United States Department of Interior Fish and Wildlife Service TN-U2-FI9AP00047. We thank two anonymous reviewers for valuable feedback on earlier versions of this manuscript.

### Appendix A. Supplementary data

Supplementary data to this article can be found online at https://doi.org/10.1016/j.biocon.2023.110181.

### References

AmphibiaWeb, 2015. Information on amphibian biology and conservation. http://amphibiaweb.org/.

Anderson, R.P., Gonzalez, I., 2011. Species-specific tuning increases robustness to sampling bias in models of species distributions: an implementation with Maxent. Ecol. Model. 222 (15), 2796–2811.

Barbet-Massin, M., Jiguet, F., Albert, C.H., Thuiller, W., 2012. Selecting pseudo-absences for species distribution models: how, where and how many? Methods Ecol. Evol. 3, 327–338.

- Basanta, M.D., Rebollar, E.A., Parra-Olea, G., 2019. Potential risk of Batrachochytrium salamandrivorans in mexico. PLoS One 14 (2), e0211960.
- Blehert, D.S., et al., 2009. Bat white-nose syndrome: an emerging fungal pathogen? Science 2009, 323–227.
- Buckley, L.B., et al., 2010. Can mechanism inform species' distribution models? Ecol. Lett. 13, 1041–1054. https://doi.org/10.1111/j.1461-0248.2010.01479.x.
- Can, Ö.E., D'Cruze, N., Macdonald, D.W., 2019. Dealing in deadly pathogens: taking stock of the legal trade in live wildlife and potential risks to human health. GECCO. https://doi.org/10.1016/j.gecco.2018e00515.
- Carter, E.D., et al., 2020. Conservation risk of Batrachochytrium salamandrivorans to endemic lungless salamanders. Conserv. Lett. 13 (1), e12675.
- Carter, E.D., et al., 2021. Winter is coming-temperature affects immune defenses and susceptibility to Batrachochytrium salamandrivorans. PloS Pathog. 17 (2) https:// doi.org/10.1371/journal.ppat.1009234.
- Cobos, M.E., Peterson, A.T., Barve, N., Osorio-Olvera, L., 2019. Kuenm: an R package for detailed development of ecological niche models using Maxent. PeerJ 7, e6281.
- DiRenzo, G.V., Grant, E.H.C., 2019. Overview of emerging amphibian pathogens and
- modeling advances for conservation-related decisions. Biol. Conserv. 236, 474–483. Elith, J., et al., 2006. Novel methods improve prediction of species' distributions from occurrence data. Ecography 29, 129–151.
- Fick, S.E., Hijmans, R.J., 2017. WorldClim 2: new 1-km spatial resolution climate surfaces for global land areas. Int. J. Climatol. 37, 4302–4315.
- Fitzpatrick, L.D., Pasmans, F., Martel, A., Cunningham, A.A., 2018. Epidemiological tracing of Batrachochytrium salamandrivorans identifies widespread infection and associated mortalities in private amphibian collections. Sci. Rep. 8 (1), 1–10.
- Fox, N., et al., 2020. "Photosearcher" package in R: an accessible and reproducible method for harvesting large datasets from Flickr. SoftwareX 12, 100624.
- Gallana, M., Ryser-Degiorgis, M.P., Wahli, T., Segner, H., 2013. Climate change and infectious diseases of wildlife: altered interactions between pathogens, vectors and hosts. Curr. Zool. 59 (3), 427–437.
- Gallant, A.L., Loveland, T.R., Sohl, T.L., Napton, D.E., 2004. Using an ecoregion framework to analyze land-cover and land-use dynamics. Environ. Manag. 34, 589–5110.
- Gascon, C., et al., 2007. Amphibian Conservation Action Plan. IUCN/SSC Amphibian Specialist Group.
- Grant, E.H., et al., 2017. Using decision analysis to support proactive management of emerging infectious wildlife diseases. Front. Ecol. Environ. 15, 214–221.
- Gray, M.J., et al., 2015. Batrachochytrium salamandrivorans: the North American response and a call for action. PLoS Pathog. https://doi.org/10.1371/journal. ppat.1005251.
- Gray, M.J., et al., 2023. Broad host susceptibility of North American amphibian species to Batrachochytrium salamandrivorans suggests high invasion potential and extinction risk. Nat. Commun. https://doi.org/10.1038/s41467-023-38979-4.
- Hijmans, R.J., Cameron, S.E., Parra, J.J., Jones, P.G., Jarvis, A., 2005. Very high resolution interpolated climate surfaces for global land areas. Int. J. Climatol. 25, 1965–1978.
- Hijmans, R.J., et al., 2013. Raster Package in R.: 2-2.
- Hill, A.J., et al., 2021. Absence of Batrachochytrium salamandrivorans in a global hotspot for salamander biodiversity. J. Wildl. Dis. 57 (3), 553–560.
  Karesh. W.B., Cook. R.A., Bennett. E.L., Newcomb. J., 2005. Wildlife trade and global
- Karesh, W.B., Cook, R.A., Bennett, E.L., Newcomb, J., 2005. Wildlife trade and global disease emergence. Emerg. Infect. Dis. 11, 1000–1002. https://doi.org/10.3201/ eid1107.020194.
- Kass, J.M., Muscarella, R., Galante, P.J., Bohl, C.L., Pinilla-Buitrago, G.E., Boria, R.A., Soley-Guardia, S., Anderson, R.P., 2023. EMMeval 2.0: redesigned for customizable and reproducible modeling of species' niches and distributions. Methods Ecol. Evol. 12, 1602–1608.
- Kembel, S.W., et al., 2010. Picante: R tools for integrating phylogenies and ecology. Bioinformatics 26, 1463–1464.
- Knutti, R., Masson, D., Gettelman, A., 2013. Climate model genealogy: generation CMIP5 and how we got there. Geophys. Res. Lett. 40, 1194–1199. https://doi.org/10.1002/grl.50256.
- Kramer-Schadt, S., et al., 2013. The importance of correcting for sampling bias iMaxEnt species distribution models. Divers. Distrib. 19 (11), 1366–1379.
- Lambert, M.R., et al., 2020. Comment on "amphibian fungal panzootic causes catastrophic and ongoing loss of biodiversity". Science 367, 6484.
- Leopardi, S., Blake, D., Puechmaille, S.J., 2015. White-nose syndrome fungus introduced from Europe to North America. Curr. Biol. 25 (6), R217–R219.
- Liaw, A., Wiener, M., 2002. Classification and regression by randomForest. R News 2 (3), 18–22.
- Lyons, M.P., Kozak, K.H., 2020. Vanishing islands in the sky? A comparison of correlation-and mechanism-based forecasts of range dynamics for montane salamanders under climate change. Ecography 43 (4), 481–493.
- Martel, A., et al., 2013. Batrachochytrium salamandrivorans sp. nov. causes lethal chytridiomycosis in amphibians. PNAS 110 (38), 15325–15329.
- Martel, A., et al., 2014. Recent introduction of a chytrid fungus endangers Western Palearctic salamanders. Science 346 (6209), 630–631.

- McNew, G.L., 1960. The nature, origin, and evolution of parasitism. In: Horsfall, J.G., Dimond, A.E. (Eds.), Plant Pathology: An Advanced Treatise. Academic Press, New York, pp. 19–69.
- Moubarak, M., Fischhoff, I.R., Han, B.A., Castellanos, A.A., 2022. A spatially explicit risk assessment of salamander populations to Batrachochytrium salamandrivorans in the United States. Divers. Distrib. https://doi.org/10.1111/ddi.13627.
- Olson, D.M., Dinerstein, E., 1998. The Global 200: a representation approach to conserving the Earth's most biologically valuable ecoregions. Conserv. Biol. 13, 502–512
- Owens, H.L., et al., 2013. Constraints on interpretation of ecological niche models by limited environmental ranges on calibration areas. Ecol. Model. 263, 10–18.
- Phillips, S., Dudik, M., 2008. Modeling of species distributions with MaxEnt: new extensions and a comprehensive evaluation. Ecography 31, 161.
- Phillips, S.J., Anderson, R.P., Schapire, R.E., 2006. Maximum entropy modeling of species geographic distributions. Ecol. Model. 190 (3–4), 231–259.
- Phillips, S.J., et al., 2009. Sample selection bias and presence-only distribution models: implications for background and pseudo-absence data. Ecol. Appl. 19 (1), 181–197.
- R Core Team, 2021. R: a language and environment for statistical computing, R Foundation for Statistical Computing, Vienna, Austria. https://www.R-project.org/.
- Refsnider, Jeanine M., et al., 2015. Genomic correlates of virulence attenuation in the deadly amphibian chytrid fungus, Batrachochytrium dendrobatidis. G3 5 (11), 2291–2298.
- Richgels, K.L., Russell, R.E., Adams, M.J., White, C.L., Grant, E.H.C., 2016. Spatial variation in risk and consequence of Batrachochytrium salamandrivorans introduction in the USA. R. Soc. Open Sci. 3 (2), 150616.
- Ripley, B., et al., 2013. "Package 'mass'." Cran r, 538, pp. 113-120.
- Rohr, J.R., et al., 2020. Towards common ground in the biodiversity-disease debate. Nat. Ecol. Evol. 4, 24–33.
- Rollins-Smith, L.A., 2020. Global amphibian declines, disease, and the ongoing battle between Batrachochytrium fungi and the immune system. Herpetologica 76 (2), 178–188.
- Scheele, B.C., et al., 2019. Amphibian fungal panzootic causes catastrophic and ongoing loss of biodiversity. Science 363 (6434), 1459–1463.
- Sessions, C., Wood, S.A., Rabotyagov, S., Fisher, D.M., 2016. Measuring recreational visitation at US National Parks with crowd-sourced photographs. J. Environ. Manag. 183, 703–711
- Siriwat, P., Nijman, V., 2020. Wildlife trade shifts from brick-and-mortar markets to virtual marketplaces: a case study of birds of prey trade in Thailand. J. Asia Pac. Biodivers. 13, 454–461. https://doi.org/10.1016/j.japb.2020.03.012.
- Stegen, G., et al., 2017. Drivers of salamander extirpation mediated by Batrachochytrium salamandrivorans. Nature 544 (7650), 353–356.
- Sutton, W.B., et al., 2015. Predicted changes in climatic niche and climate refugia of conservation priority salamander species in the northeastern United States. Forests 6 (1), 1–26.
- Tingley, R., Vallinoto, M., Sequeira, F., Kearney, M.R., 2014. Realized niche shift during a global biological invasion. PNAS 111, 10233–10238. https://doi.org/10.1073/ pnas.1405766111.
- Tornabene, B.J., et al., 2018. The influence of landscape and environmental factors on ranavirus epidemiology in a California amphibian assemblage. Freshw. Biol. 63, 639–651.
- van Vuuren, D.P., et al., 2011. The representative concentration pathways: an overview. Clim. Chang. 109, 5–31.
- Venesky, M.D., Liu, X., Sauer, E.L., Rohr, R., 2014. Linking manipulative experiments to field data to test the dilution effect. J. Anim. Ecol. 83, 557–565.
- Waddle, J.H., et al., 2020. Batrachochytrium salamandrivorans (Bsal) not detected in an intensive survey of wild North American amphibians. Sci. Rep. 10 (1), 1–7.
- Wake, D.B., Vredenburg, V.T., 2008. Are we in the midst of the sixth mass extinction? A view from the world of amphibians. PNAS 105, 11466–11473.
- Walker, S.F., et al., 2008. Invasive pathogens threaten species recovery programs. Curr. Biol. 18, R853–R854.
- Warren, D.L., Seifert, S.N., 2011. Ecological niche modeling in Maxent: the importance of model complexity and the performance of model selection criteria. Ecol. Appl. 21, 335–342.
- Wisz, M.S., et al., 2008. Effects of sample size on the performance of species distribution models. Divers. Distrib. 14, 763–773.
- Wood, S.A., Guerry, A.D., Silver, J.M., Lacayo, M., 2013. Using social media to quantify nature-based tourism and recreation. Sci. Rep. 3 (1), 1–7.
- Wright, A.N., Hijmans, R.J., Schwartz, M.W., Shaffer, H.B., 2015. Multiple sources of uncertainty affect metrics for ranking conservation risk under climate change. Divers. Distrib. 21 (1), 111–122.
- Xie, G.Y., Olson, D.H., Blaustein, A.R., 2016. Projecting the global distribution of the emerging amphibian fungal pathogen, Batrachochytrium dendrobatidis, based on IPCC climate futures. PLoS One 11 (8), e0160746.
- Yap, T.A., Koo, M.S., Ambrose, R.F., Wake, D.B., Vredenburg, V.T., 2015. Averting a north American biodiversity crisis. Science 349 (6247), 481–482.